Arch. Metall. Mater. **63** (2018), 2, 709-717

DOI: 10.24425/122397

E. RUDNIK*#, M. KOSTĘPSKI*

COMPARATIVE STUDIES ON THE CODEPOSITION OF ANTIMONY AND TIN FROM ACIDIC CHLORIDE AND SULFATE-CHLORIDE SOLUTIONS

Codeposition of antimony and tin from acidic chloride and chloride-sulfate baths was investigated. The calculations of distribution of species showed domination of neutral $SnCl_2$ and anionic $SbCl_4^-$ complexes in chloride solution, while in the presence of sulfate ions neutral $SnSO_4$ and cationic $SbCl^{2+}$ complexes were found. Cyclic voltammetry, anodic stripping analysis and potentiostatic measurements showed that antimony deposited favorably and the reaction run under limiting control. Analysis of chronoamperometric curves suggested instantaneous nucleation of the solid phase in the chloride bath, but progressive model was more probable in the presence of sulfate ions.

Keywords: antimony; electrolysis; speciation; tin; voltammetry

1. Introduction

In recent years there is a growing interest in the research on new materials for anodes in lithium-ion batteries [1]. Tin-based alloys are the most important alternatives for graphite anode as metallic tin can react electrochemically with lithium at room temperature forming various lithium-rich intermetallic phases [1-4]. These can yield a maximum theoretical capacity up to ~990 mAh/g, while for graphite this value reaches ~370 mAh/g. However, incorporation of large amounts of lithium is associated with serious changes of the material volume during cyclic charge/discharge. Various studies have shown that stability of Li_xSn_y phases may be improved by replacement of pure tin by tin alloys or intermetallic compounds [3,4]. Additional constituent may be active or unreactive towards lithium, but it serves as a matrix buffering the volume change of the active tin phase during Li insertion-extraction steps. It results in less cracking, enhanced cyclability and higher capacities of the anode material due to formation of specific intermetallic compounds. It was shown that Sn-Sb system provides favorable properties as it comprises two active Li_xSb compounds resulting in the increased capacity of the anode [2-5].

Sn-Sb material for Li-ions batteries can be fabricated using various techniques [1,6] although electrodeposition seems to be the most attractive. The most important advantages of the process are: the possibility of deposition of metals and alloys on substrates of large/small areas; ability to accurate control the processes taking place during the electrodeposition (monitoring of the composition, grain size, thickness of deposits etc.); deposition of three-dimensional structures of controlled architecture; high purity of the final product; application of cheap and available reagents; no need to incur high costs of maintaining a vacuum or high temperatures; no toxic by-products generation during electrolysis; easy regeneration of waste solutions and the feasibility of realization in industrial scale. A review of the literature data on the electrodeposition of Sn-Sb alloys is rather meager. Brenner [7] and Sadana et al. [8] presented summarized data on the deposition of antimony and its alloys. Several baths have been proposed for the codeposition of antimony and tin. These are mainly: acid fluoride [7,8] or alkaline tartrate [9] and pyrophosphate-tartrate [5,10,11] baths. Acid sulfate electrolytes with various organic additives [12,13] and nonaqueous systems [14,15] were also proposed. It was shown that although the alloys can be deposited from both acid and alkaline solutions, acid fluoride baths were found as more practical for the application [7,8]. In such solutions both metal ions form fluoride complexes and from the baths of high Sb(III):Sn(II) ratio antimony deposits less readily than tin forming alloys with the composition not sensitive to the current density [7]. Fluoride baths operate at high temperature (65°C) [7,8] and can make corrosion problems caused by free hydrogen fluoride. Therefore aggressive fluoride-chloride solutions are often replaced by less corrosive baths based on the tartrate complexes of tin and antimony. In such cases a mixture of tin and SnSb phase was detected in the electrodeposits [11].

In the previous papers detailed electrochemical studies on the deposition of tin [16,17] and tin-nickel alloys [18, 19] from acidic solutions were presented. The aim of the present paper was to determine the influence of sulfate ions on the codeposition of tin and antimony from acid chloride solutions containing

* AGH UNIVERSITY OF SCIENCE AND TECHNOLOGY, FACULTY OF NON – FERROUS METALS, DEPARTMENT OF PHYSICAL CHEMISTRY AND METALLURGY OF NON-FERROUS METALS, AL. MICKIEWICZA 30, 30-059 KRAKÓW, POLAND

Corresponding author: erudnik@agh.edu.pl

gluconate and borate ions. Electrodeposition of the alloys was discussed in terms of electrochemical analysis of the process using cyclic voltammetry, anodic stripping and chronoamperometry as similar investigation of Sb and Sn codeposition was not presented in the literature yet.

2. Experimental

Investigations of tin and antimony codeposition were carried out from two baths containing: 50 mM tin(II) chloride $SnCl_2$, 50 mM antimony(III) chloride $SbCl_3$, 0.5 M boric acid H_3BO_3, 0.2 M sodium gluconate $C_6H_{11}O_7Na$ and 0.5 M ammonium salt chloride NH_4Cl or sulfate $(NH_4)_2SO_4$. pH of the baths was 0.2 ± 0.1. Reagents of analytical purity were used.

Electrochemical measurements were carried out in a three-electrode cell using a glassy carbon (GC) working electrode (0.196 cm^2), a platinum plate (2 cm^2) as a counter electrode and an $Ag/AgCl/KCl_{sat}$ electrode as a reference electrode (all potentials are referred to this electrode). Potentiostatic deposition (10 min. at potentials from –0.1V to –0.7V) was performed in the same system, but α-brass (10wt% Zn) plates (0.785 cm^2) as cathode substrates were used. Before each experiment the glassy carbon electrode with a mirror finish was chemically cleaned, while brass sheets were chemically polished in a mixture of concentrated acids (HNO_3:H_3PO_4:CH_3COOH with 1:3:1 volume ratio). Solution volume of 20 cm^3 was used in each electrochemical test. Morphology of the layers was examined under optical microscope (Nikon). Chemical composition of the deposits was determined (in wt%) by XRF analyzer (Rigaku). Structure of the deposits was analyzed by X-ray diffractometry (Rikagu, $Cu_{K\alpha}$ radiation).

Cyclic and anodic stripping voltammograms were registered at a potential scan rate of 10 $mV \cdot s^{-1}$. First CV sweep was always performed from the initial potential of 0.5 V (Ag/AgCl) towards more negative values. Stripping analysis was performed immediately after potentiostatic deposition (for 40 s) at fixed potential without removing the working electrode from the solution. Anodic stripping curves were registered from deposition potentials up to 0.5 V. Nucleation of solid phase was investigated using chronoamperometry realized at various constant potentials for 15 s.

Autolab potentiostat/galvanostat (PGSTAT30) controlled by a microcomputer was applied in all measurements. All experiments were performed at room temperature. No bath agitation was used.

3. Results and discussion

3.1. Electrolyte speciation

Divalent tin and trivalent antimony ions are present in aqueous solutions as free ions as well as neutral and/or charged complexes with formulas dependent on the salt type and solution pH. Specific distribution of the individual species is governed mainly by total concentrations of ions, type and concentration of other compounds added to the bath, pH and temperature, but in Sn(II) and Sb(III) systems high tendency of the salts for hydrolysis should be emphasized [20]. E-pH diagram for Sn-H_2O system [21] for ionic species concentration 10^{-2} M shows the predominance of Sn^{2+} simple ion in the solutions with pH below 1 due to easy formation of sparingly soluble basic salts in less acidic conditions. For example, in chloride baths SnOHCl precipitates are detected in preference to any other oxide (e.g. SnO). Dissolution of antimony(III) salts in water is more complicated process and stable soluble SbO^+ (or $Sb(OH)_2^+$) form exists in 10^{-2} M solutions for pH below -1 [20,21]. Hydrolysis reaction of metal ions results in the formation of basic chlorides: SbOCl in concentrated solutions and $Sb_4O_5Cl_2$ in more dilute baths. Hydrolysis of tin and antimony salts may be inhibited by the complexation of ions. Tin(II) ions combining with gluconate or chloride ions produce soluble complexes [16,17,20], while for antimony(III) only chloride ions are suitable [20]. The latter was qualitatively confirmed by the authors during preparation of the sulfate-gluconate solution. Addition of gluconate ions as well as strong acidification of the electrolyte with sulfuric acid were not able to dissolve secondary precipitate of antimony(III). Literature data shows that at Sb(III) concentrations above 0.1 mM a polymerization of antimony(III) species in sulfate solutions occurs [20].

Composition of the electrolyte determines speciation of the solution. In this research work acid chloride-gluconate and chloride-sulfate-gluconate solutions were used, hence species presented in Table 1 were taken into account over the pH range from –2 to 2. It should be noted that a number of equilibrium constants for the formation of tin(II) complexes can be found in the literature, while that for antimony(III) reported values show a spread. Tin(II) forms a variety of complexes with chloride ions, including mixed tin(II) chloride-hydroxide species. Antimony(III) forms complexes with chloride ions in acid solutions and experimental evidence confirms that Sb(III) chloride complexes are important only in very acid solution at pH below 2, while under other conditions, hydrolyzed species are dominant [20]. The formation of $SbOSO_4^-$ in 2-6 M H_2SO_4 solutions and $Sb(SO_4)_2^-$ complexes in 14-16 M H_2SO_4 solutions was also proposed in the literature. No stability constants for the Sb(III) sulfate complexes are proposed in this research, since such complexes, seems to be important only in concentrated sulfate solutions.

Using equilibrium quotients assigned to the reactions listed in Table 1 and HySS2009 software pH-dependent distributions of species at total concentrations of the components used in this study were calculated and presented in Fig. 1. Specific compositions of the solutions are rather complicated due to formation of a variety of tin(II) and antimony(III) compounds. In chloride solutions concentrations of the individual species are practically unchanged for pH below 1 and neutral $SnCl_2$ and anionic $SbCl_4^-$ complexes predominate. Addition of sulfate ions to the chloride system seriously changes speciation of the Sn(II)-Sb(III) system, which is more affected by pH changes in the acid range. In this

TABLE 1

Equilibrium constants for formation of various Sn(II) and Sb(III) species

Reaction	Equilibrium quotient	Constant	Ref.
$Sn^{2+} + H_2O \leftrightarrow SnOH^+ + H^+$	$\beta_1 = \frac{[SnOH^+][H^+]}{[Sn^{2+}]}$	$\log \beta_1 = -3.75$	[20]
$Sn^{2+} + 2H_2O \leftrightarrow Sn(OH)_2 + 2H^+$	$\beta_2 = \frac{[Sn(OH)_2][H^+]^2}{[Sn^{2+}]}$	$\log \beta_2 = -7.71$	
$Sn^{2+} + 3H_2O \leftrightarrow Sn(OH)_3^- + 3H^+$	$\beta_3 = \frac{[Sn(OH)_3^-][H^+]^3}{[Sn^{2+}]}$	$\log \beta_3 = -17.54$	
$Sn^{2+} + H_2O \leftrightarrow SnO_s + 2H^+$	$K_{SO1} = [Sn^{2+}]^{-1}[H^+]^2$	$\log K_{S01} = -2.41$	
$Sn^{2+} + Cl^- \leftrightarrow SnCl^+$	$\beta_4 = \frac{[SnCl^+]}{[Sn^{2+}][Cl^-]}$	$\log \beta_4 = 1.65$	
$Sn^{2+} + 2Cl^- \leftrightarrow SnCl_2$	$\beta_5 = \frac{[SnCl_2]}{[Sn^{2+}][Cl^-]^2}$	$\log \beta_5 = 2.31$	
$Sn^{2+} + 3Cl^- \leftrightarrow SnCl_3^-$	$\beta_6 = \frac{[SnCl_3^-]}{[Sn^{2+}][Cl^-]^3}$	$\log \beta_6 = 2.09$	
$Sn^{2+} + Cl^- + H_2O \leftrightarrow SnOHCl$	$\beta_7 = \frac{[SnOHCl]}{[Sn^{2+}][Cl^-]}$	$\log \beta_7 = -2.27$	
$Sn^{2+} + Cl^- + H_2O \leftrightarrow SnOHCl_s$	$K_{SO2} = [Sn^{2+}]^{-1}[Cl^-]^{-1}$	$\log K_{S02} = 2.42$	
$Sn^{2+} + SO_4^{2-} \leftrightarrow SnSO_4$	$\beta_8 = \frac{[SnSO_4]}{[Sn^{2+}][SO_4^{2-}]}$	$\log \beta_8 = 2.91$	
$Sn^{2+} + 2SO_4^{2-} \leftrightarrow Sn(SO_4)_2^{2-}$	$\beta_9 = \frac{[Sn(SO_4)_2^{2-}]}{[Sn^{2+}][SO_4^{2-}]^2}$	$\log \beta_9 = 2.83$	
$Sn^{2+} + Glu^- \leftrightarrow SnGlu^+$	$\beta_{10} = \frac{[SnGlu^+]}{[Sn^{2+}][Glu^-]}$	$\log \beta_{10} = 3.01$	[22]
$Sn^{2+} + 2Glu^- \leftrightarrow SnGlu_2$	$\beta_{11} = \frac{[SnGlu_2]}{[Sn^{2+}][Glu^-]^2}$	$\log \beta_{11} = 5.29$	
$Sb^{3+} + Cl^- \leftrightarrow SbCl^{2+}$	$\beta_{12} = \frac{[SbCl^{2+}]}{[Sb^{3+}][Cl^-]}$	$\log \beta_{12} = 3.51$	[20]
$Sb^{3+} + 2Cl^- \leftrightarrow SbCl_2^+$	$\beta_{13} = \frac{[SbCl_2^+]}{[Sb^{3+}][Cl^-]^2}$	$\log \beta_{13} = 4.00$	
$Sb^{3+} + 3Cl^- \leftrightarrow SbCl_3$	$\beta_{14} = \frac{[SbCl_3]}{[Sb^{3+}][Cl^-]^3}$	$\log \beta_{14} = 4.09$	
$Sb^{3+} + 4Cl^- \leftrightarrow SbCl_4^-$	$\beta_{15} = \frac{[SbCl_4^-]}{[Sb^{3+}][Cl^-]^4}$	$\log \beta_{15} = 4.72$	
$Sb^{3+} + 5Cl^- \leftrightarrow SbCl_5^{2-}$	$\beta_{16} = \frac{[SbCl_5^{2-}]}{[Sb^{3+}][Cl^-]^5}$	$\log \beta_{16} = 4.72$	
$Sb^{3+} + 6Cl^- \leftrightarrow SbCl_6^{3-}$	$\beta_{17} = \frac{[SbCl_6^{3-}]}{[Sb^{3+}][Cl^-]^6}$	$\log \beta_{17} = 4.11$	
$Sb^{3+} + 3H_2O \leftrightarrow Sb(OH)_3 + 3H^+$	$\beta_{18} = \frac{[Sb(OH)_3][H^+]^3}{[Sb^{3+}]}$	$\log \beta_{18} = 0.73$	
$Sb(OH)^{2+} + 2H_2O \leftrightarrow Sb(OH)_3 + 2H^+$	$\beta_{19} = \frac{[Sb(OH)_3][H^+]^2}{[Sb(OH)^{2+}]}$	$\log \beta_{19} = -0.83$	
$Sb(OH)_2^+ + H_2O \leftrightarrow Sb(OH)_3 + H^+$	$\beta_{20} = \frac{\left[Sb(OH)_3\right]\left[H^+\right]}{\left[Sb(OH)_2^+\right]}$	$\log \beta_{20} = -1.30$	
$2Sb(OH)_3 \leftrightarrow \alpha\text{-}Sb_2O_{3\,s} + 2H_2O$	$K_{SO3} = [Sb(OH)_3]^{-2}$	$\log K_{S03} = 8.32$	
$2Sb(OH)_3 + Cl^- + H^+ \leftrightarrow SbOCl_s + 2H_2O$	$K_{SO4} = [Sb(OH)_3]^{-2}\left([Cl^-][H^+]\right)^{-1}$	$\log K_{S04} = 1.80$	
$H^+ + SO_4^{2-} \leftrightarrow HSO_4^-$	$K_{a1} = \frac{[HSO_4^-]}{[H^+][SO_4^{2-}]}$	$\log K_{a1} = 1.12$	[23]
$H^+ + Glu^- \leftrightarrow HGlu$	$K_{a2} = \frac{[HGlu]}{[H^+][Glu^-]}$	$\log K_{a2} = 3.56$	

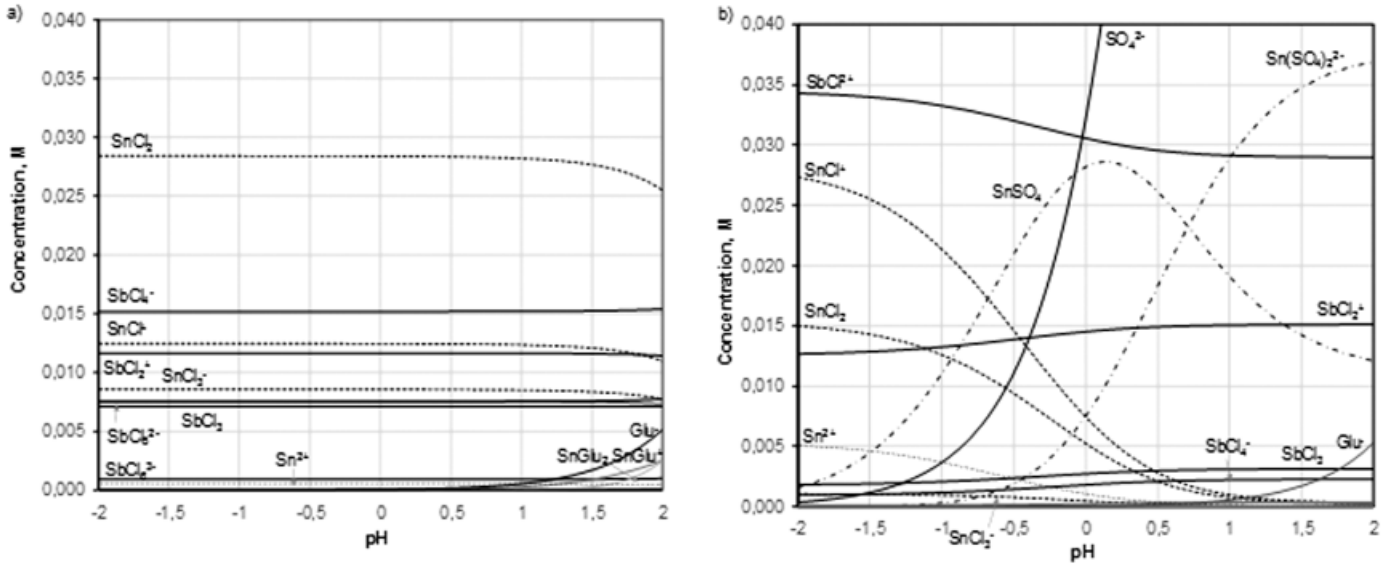

Fig. 1. Distribution of species in Sn(II)-Sb(III) solutions: a) chloride, b) chloride-sulfate (total ions concentrations as used in this study)

case neutral $SnSO_4$ and cationic $SbCl^{2+}$ complexes dominate at pH of 0.2 used in this work. Low amounts of Sn(II)-gluconate compounds appear at less acidic conditions (pH above 1.5) in the chloride bath, but not in the chloride-sulfate due to higher affinity of Sn(II) to the formation of anionic sulfate complex. In both cases various hydroxy-complexes show negligible fractions of total Sn(II) and Sb(III) amounts and no precipitation of sparingly soluble compounds is predicted despite of low solubility products of basic salts or hydrated oxides in the considered pH range.

3.2. Cyclic voltammetry

Cyclic voltammograms registered in the solutions were started from 0.5 V, then potential was scanned to the negative direction and reversed at various potentials. Fig. 2 and Fig. 3 show exemplary curves registered for the chloride and chloride-sulfate solution, respectively. It was observed that electrodeposition of metal directly on the glassy carbon electrode started suddenly at potentials below –0.27 V (vs. Ag/AgCl). It corresponded to the

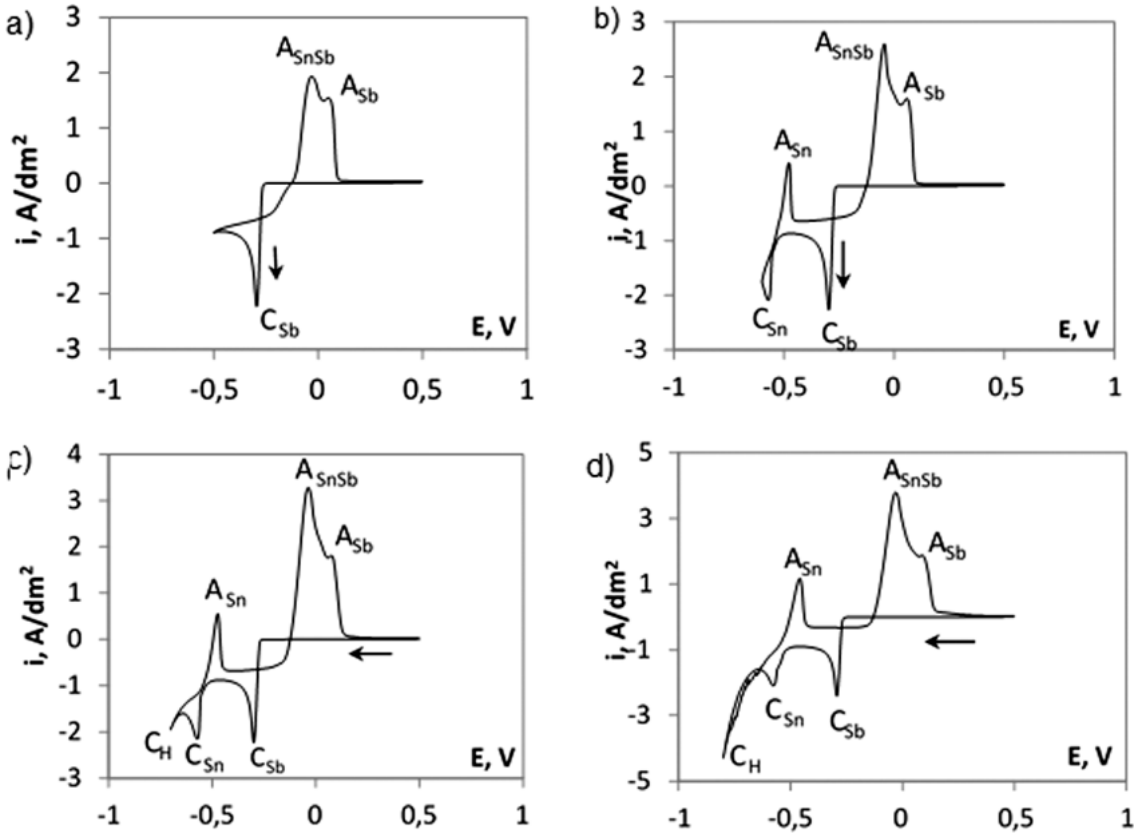

Fig. 2. Cyclic voltammetry curves registered in the chloride solution at various vertex potentials: a) –0.5 V; b) –0.6 V; c) –0.7 V; d) –0.8 V

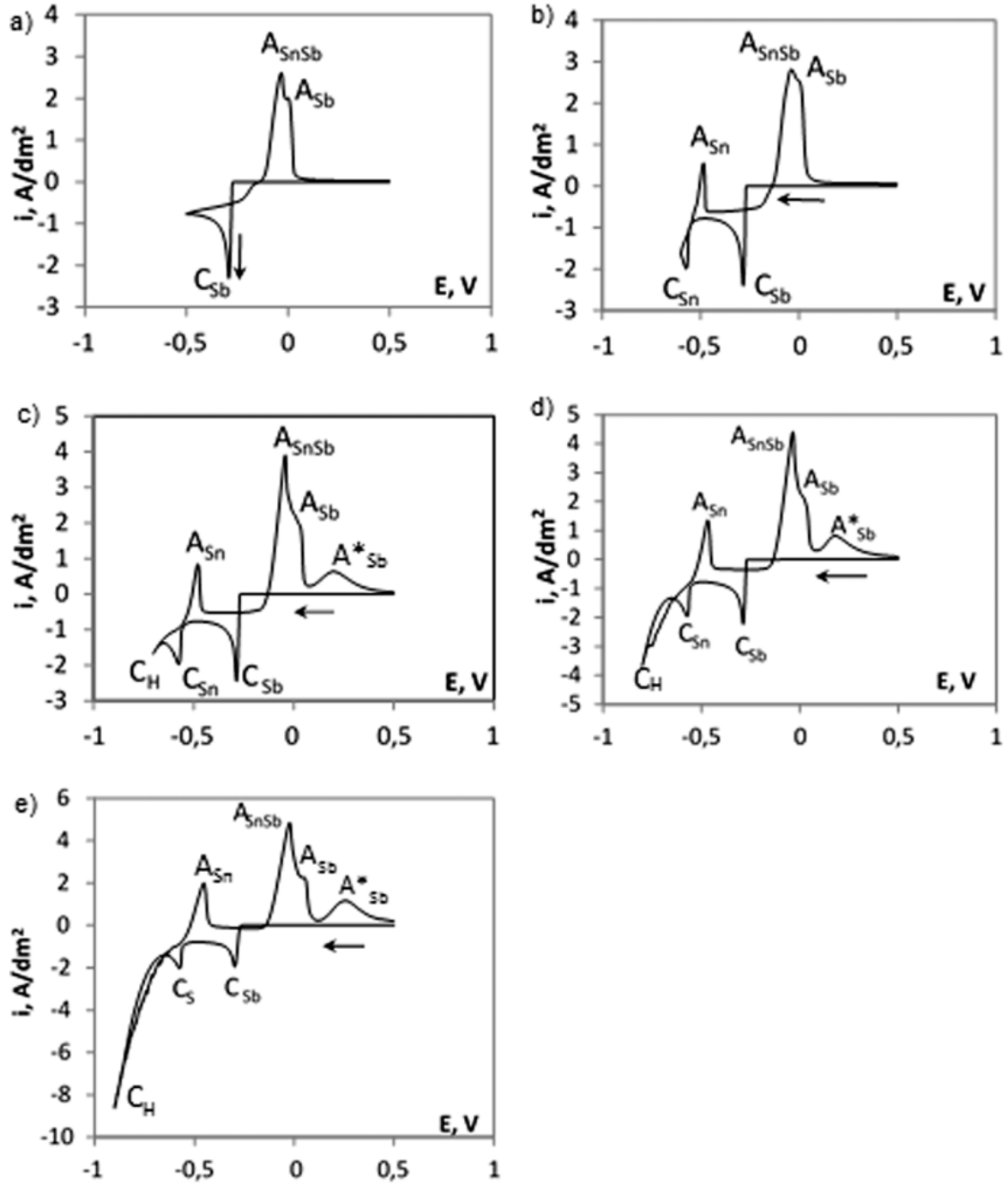

Fig. 3. Cyclic voltammetry curves registered in the chloride-sulfate solution at various vertex potentials: a) –0.5V; b) –0.6V; c) –0.7V; d) –0.8 V

antimony deposition (C_{Sb}) as more noble element. Further sweep of the potential towards electronegative values was accompanied by cathodic process running under limiting current followed by the cathodic peak of tin ions reduction at –0.57 V (C_{Sn}) and hydrogen evolution below –0.67 V (C_H). During reverse scan two characteristics crossovers between the branches for the negative and positive sweeps were observed: at –0.25 V and –0.55 V for antimony and for tin deposition, respectively. They formed loops typical for the nucleation and growth of a new phase. The cathodic currents were higher during the reverse sweep than during the forward sweep for each bath. It is obvious, since energy required for metal overpotential deposition on the foreign substrate is higher than that for the metal deposition on the native layer formed during the previous scan [24]. Comparison of the potential ranges of the cathodic reactions showed similar behavior, independently on the type of the bath.

Differences in the voltammetric curves were found during reverse sweeps. Three anodic peaks were detected in both systems corresponding to anodic dissolution of tin at –0.49 V (A_{Sn}), pure antimony at 0.08 V (A_{SnSb}) and Sn-Sb phase at –0.03 V (A_{SnSb}). The latter was close to the antimony anodic peak indicating formation of Sn-Sb phase enriched in antimony. Moreover, the height of A_{SnSb} peak increased as the vertex potential was more cathodic (enhanced tin and antimony codeposition), while

the antimony anodic peak A_{Sb} remained practically unchanged due to the antimony deposition under diffusion control (with constant deposition rate) during the forward sweep. In the presence of sulfate ions additional wide anodic peak was raised at 0.22 V (A^*_{Sb}), but only if the vertex potential was –0.7 V and below. For such potential range intense hydrogen evolution was observed (up to 8.5 A/dm^2 for –0.9 V). It favours hydrolysis of antimony(III), especially at low concentration of chloride complexing ions. Therefore, it is believed that A^*_{Sb} corresponds to the oxidation of some Sb(III) hydrolysis product, especially that the height of this peak increased from 0.8 A/dm^2 to 1.14 A/dm^2 with decreased vertex potential. Similar anodic peak was not observed in the chloride solution, where concentration of Cl^- was enough to prevent any secondary reactions at the cathode surface.

3.3. Anodic stripping voltammetry

Fig. 4 shows anodic peaks representing a part of stripping voltammograms registered for various deposition potentials. Results of anodic stripping confirm the data presented for cyclic voltammetry. Three main anodic peaks were obtained, independently on the bath composition and deposition potential. As previously, codeposition of the metals from the chloride-sulfate solution at potentials lower than –0.6 V produced new anodic peak A^*_{Sb}. Decrease in the deposition potential was accompanied by the shift of the anodic peak towards more electronegative direction. It shows that increased hydrogen evolution during potentiostatic deposition at lower potentials favors precipitation of hydrolysed forms of antimony, thus broad peak corresponding to the oxidation of some hydroxide compound becomes more narrow and higher as the amount of the co-precipitated species increases. An interesting fact was also observed in this solution. At the potential of –0.4 V only antimony was deposited, and single anodic peak was observed A_{Sb}, but at more negative potentials tin started to deposit resulting in the formation not only pure phase A_{Sn}, but also Sn-Sb phase rich in antimony. The latter resulted in the shift of the A_{Sb} maxima towards more negative potentials (marked then as A_{Sn-Sb}).

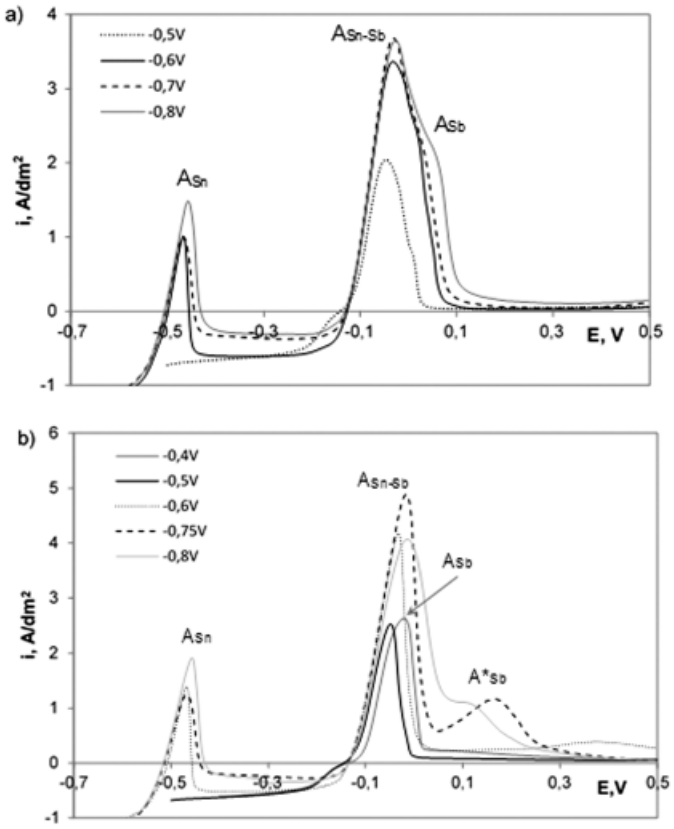

Fig. 4. Anodic stripping voltammetry curves registered in the solutions: a) chloride, b) chloride-sulfate. Former deposition time: 40 s

3.4. Chronoamperometry

The initial stage of Sn-Sb codeposition on the glassy carbon was studied by means of potentiostatic step technique. Glassy carbon was used to prevent hydrogen evolution and to avoid precipitation of secondary products of antimony. Fig. 5 shows current transients recorded for the baths at various deposition potentials from the range of simultaneous reduction of both ions (i.e. below –0.5V for 15 s). The curves show a gradual increase of the cathodic current up to a maximum for all potentials (at shorter

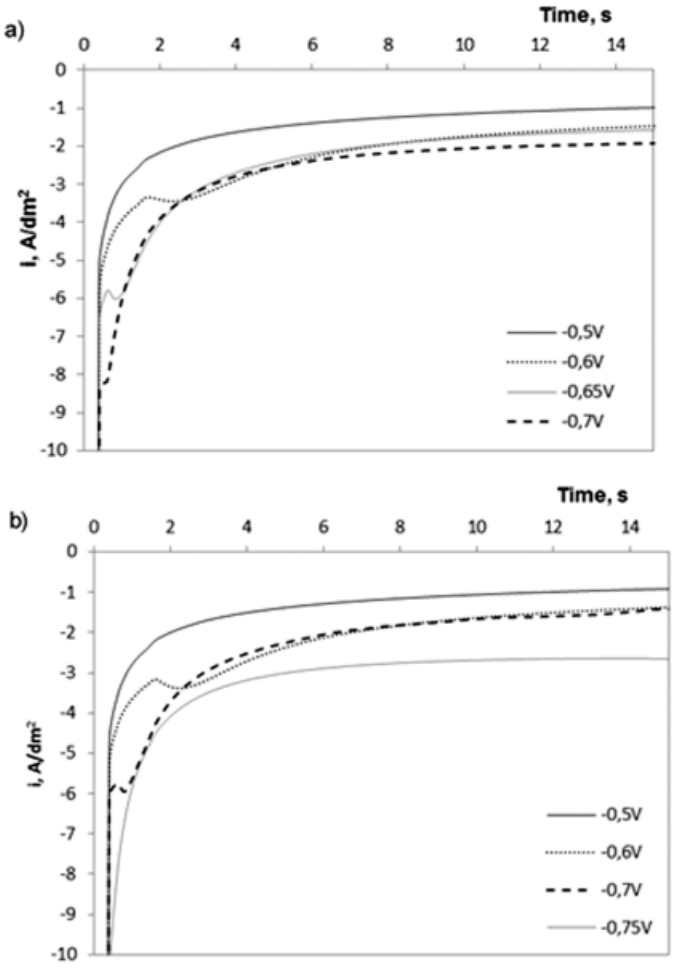

Fig. 5. Chronoamperometric transients registered in the solutions: a) chloride, b) chloride-sulfate

times for more negative potentials) with their final part falling to the plateau. The course of the *I-t* transients is typical for the response of a three-dimensional nucleation and growth process occurring under the mass transfer control [24]. It is consisted with the voltammetric curves presented in Fig. 2, which show that reduction of antimony ions run under diffusion control at potentials below –0.4 V. The rise of the current in the *I-t* plots corresponds to the increase of the electroactive area due to the growth of the individual isolated nuclei and/or the increase of the number of nuclei. At this step transport of the ionic species to the growing centers occurs through hemispherical diffusion zones formed around each isolated nucleus. Radii of the hemispherical zones increase with time and the diffusion zones start to overlap forming finally a planar diffusion layer [25]. The maximum of the cathodic current at short times is related to the maximal electroactive area, i.e. the moment at which hemispherical metal nuclei are on the point of the collision. The current then falls and the transients are characterized by the Cottrell equation, since the electrochemical reaction run under linear diffusion. However, simultaneous deposition of two metals may disturb general behavior described by the model developed for single metal ions reduction, caused by various diffusion coefficients as example. Despite of this a trial of the analysis of the Sn-Sb phase formation was performed.

The position of cathodic current maxima in chronoamperometric curves was not seriously dependent on the bath composition, but in the presence sulfate ions maxima $(i/i_{max})^2$ are at little longer times. Despite of that a general behavior was observed as the deposition potential was more cathodic the current reached its maximal value at shorter times.

Theory of the potentiostatic current transients for three-dimensional multiple nucleation with diffusion controlled growth was discussed by various authors [24]. Mathematical model for instantaneous and progressive nucleation developed by Sharifker and Hills [25] has been successfully used to analyze the current transients of pure metal deposition [16,17]. A classification of the nucleation type is possible by comparison of the experimental results with the theoretical curves plotted in a dimensionless form. In the case of instantaneous nucleation all nuclei are generated simultaneously and they grow further with the same rate. Under these conditions the following diagnostic equation is satisfied [25]:

$$\left(\frac{I}{I_{max}}\right)^2 = \frac{1.9542}{\frac{t}{t_{max}}}\left[1-\exp\left(-1.2564\frac{t}{t_{max}}\right)\right]^2 \qquad (1)$$

During progressive nucleation the nuclei are formed constantly and they grow to different sizes and/or at different rates. In such case appropriate expression is as follows:

$$\left(\frac{I}{I_{max}}\right)^2 = \frac{1.2254}{\frac{t}{t_{max}}}\left[1-\exp\left(-2.3367\left[\frac{t}{t_{max}}\right]^2\right)\right]^2 \qquad (2)$$

Fig. 6 shows a comparison of non-dimensional plots for instantaneous and progressive nucleation models with the experimental data. It was observed that at t/t_{max} closed to 1 for the transients in the chloride bath showed a behavior corresponding to an instantaneous nucleation, while in the presence of sulfate anions a progressive nucleation was more emphasized. This shows that sulfate ions inhibit formation of the nuclei, which is often ascribed to the adsorption of sulfate ions on the cathode surface. For $t/t_{max} > 2$ a deviation from the predicted curves appeared caused probably by reduction of antimony species limited by diffusion.

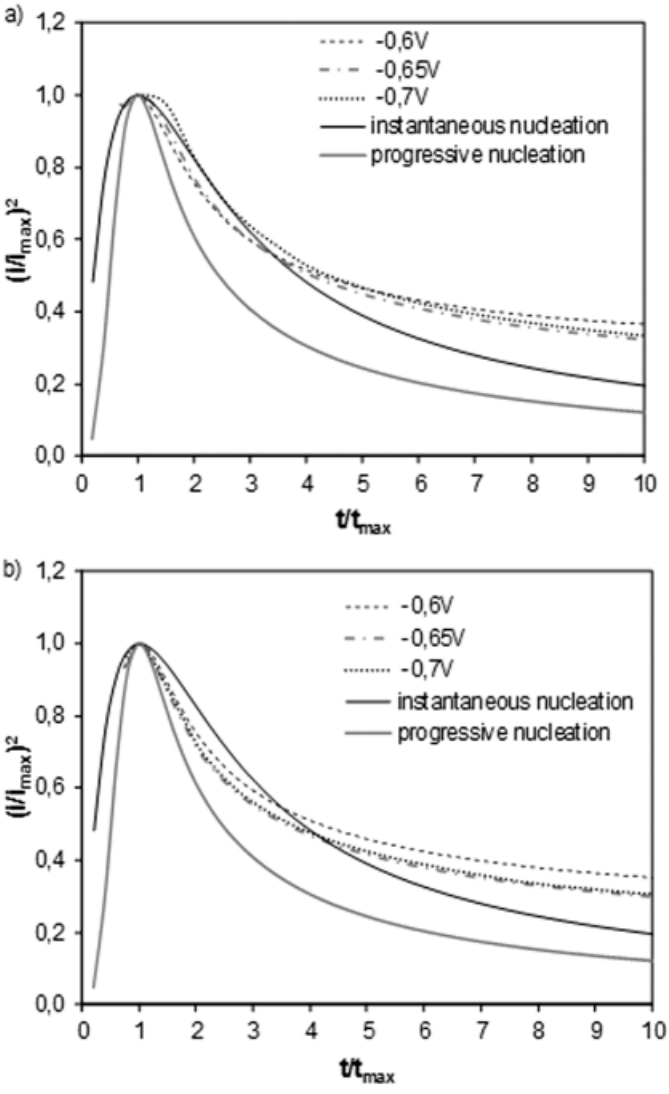

Fig. 6. Non-dimensional plots for instantaneous and progressive nucleation models and experimental data: a) chloride solution, b) chloride-sulfate solution

Recently, Díaz-Morales et al. [26] developed a model describing the kinetics of nucleation and diffusion-controlled growth of bimetallic phases. It assumed that the volumes of the pure components are additive in the bimetallic deposit, as in ideal solutions. The equation for the current transient was obtained using an approach similar to that used for the nucleation and growth of pure metals [25] discussed above.

3.5. Potentiostatic deposition

Tin and antimony were deposited on the brass substrate. Obtained results are consistent with the voltammetric data. Rough or porous, gray deposits were obtained (Fig. 7). Antimony layers were produced from chloride solutions at the potentials –0.6 V and above and from chloride-sulfate solutions at the potentials –0.5 V and more positive. Codeposition of the metals was observed at –0.7 V in the chloride bath (6%Sn-94%Sb) as well as at –0.6 V (23.7%Sn-76.3%Sb) and –0.7 V (40.3%Sn-59.7%Sb) in the chloride-sulfate solution.

Diffraction patterns of the coatings are shown in Fig. 8. The main component of all deposits was antimony (trigonal) contaminated by antimony oxide Sb_2O_3, probably as secondary product. It was also observed as white precipitates on the surface of the deposits (Fig. 7b,c). In some cases peaks characteristic for tin were found. However no Sn-Sb phases (cubic or trigonal) were detected despite that tin-antimony was identified previously during electrochemical analysis of the deposits. However, it should be noted that diffractograms for the deposits produced at the potential –0.6V changed in comparison to the results obtained at more positive potentials. It suggests formation of the

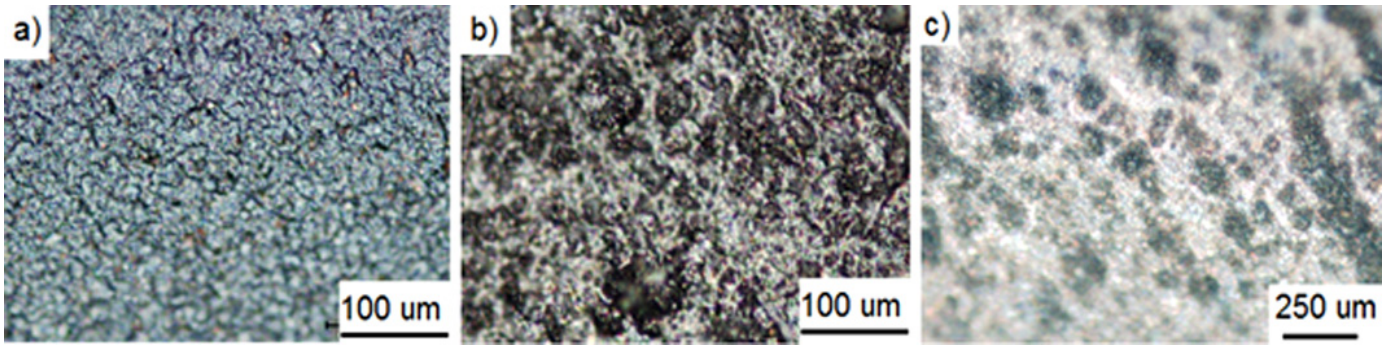

Fig. 7. Surface morphology of deposits obtained: a) –0.1 V in chloride bath, b) –0.6 V in chloride bath, c) –0.6 V in chloride-sulfate bath

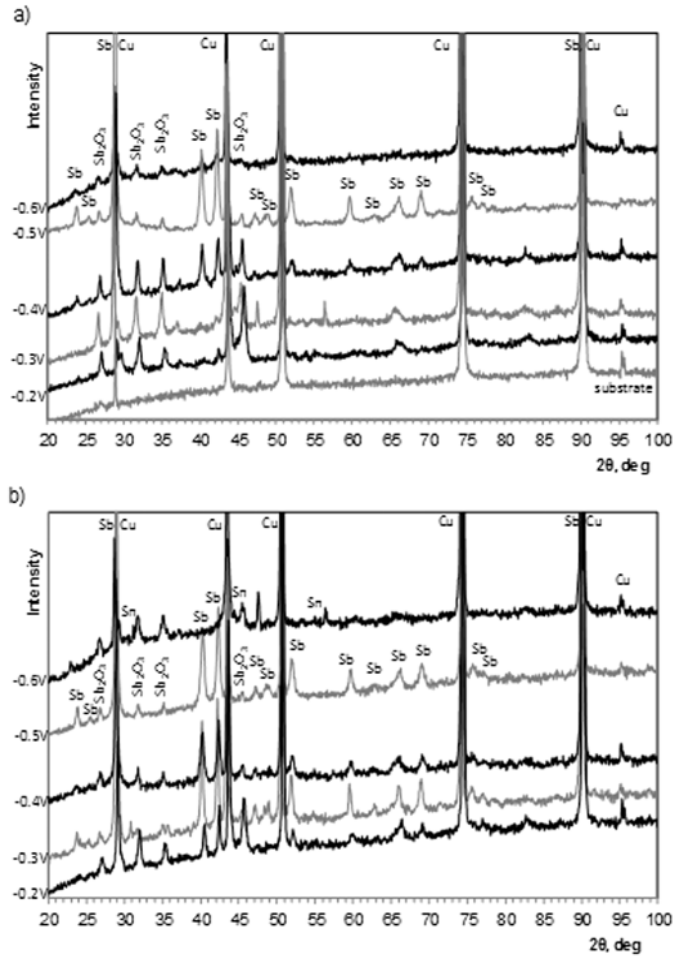

Fig. 8. X-ray diffraction patterns of deposits produced in the solutions: a) chloride, b) chloride-sulfate

deposits with very fined grains making difficult identification of their phase crystalline structure.

Current efficiency of the cathodic process was calculated. For codeposition of the metals theoretical mass of the deposit was found from the following equation:

$$m = \frac{Q \cdot 100\%}{F\left(\frac{2 \cdot \%\mathrm{Sn}}{M_{\mathrm{Sn}}} + \frac{3 \cdot \%\mathrm{Sb}}{M_{\mathrm{Sb}}}\right)} \tag{3}$$

It includes weight percentages of tin and antimony (%Sn, %Sb) in the layers, molar masses of the elements (M_{Sn}, M_{Sb}), total charge flowed through the cathode during electrolysis (Q). The obtained values for pure antimony deposition from the chloride solution were rather low, in the range of 20-29%, while in the presence of sulfate ions they increased to 51-80%. However, in both cases no general tendency was observed with the decreased cathodic potential due to formation of porous deposits contaminated by secondary product. Current efficiency of the Sn-Sb codeposition from the chloride bath (–0.7 V) was 11%, but in the chloride-sulfate solution it increased to 32% and 92% for the deposition potential of –0.6 V and –0.7 V, respectively.

4. Conclusions

Electrodeposition of antimony and tin from acidic chloride and chloride-sulfate baths was investigated. Distribution of species showed domination of neutral $SnCl_2$ and anionic $SbCl_4^-$ complexes in chloride solution, while in the presence of sulfate

ions neutral $SnSO_4$ and cationic $SbCl^{2+}$ complexes dominated. Cyclic voltammetry, anodic stripping analysis and potentiostatic measurements showed that antimony deposited predominantly as more noble component and the reaction occurred under limiting control resulting in the formation of porous deposits. This shows that despite of formation Sn(II) and Sb(III) complexes in the electrolytes both metals behave as in the simply salt solutions. Analysis of chronoamperometric curves suggested instantaneous nucleation of the solid phase in the chloride bath, but progressive model was more probable in the presence of sulfate ions.

Acknowledgements

This work was realized under AGH-UST research project No. 11.11.180.654.

REFERENCES

[1] Y. Wu, Lithium-ion batteries: fundamentals and application, CRC Press, Boca Raton, 2015.
[2] W.J. Zhang, J. Power Sourc. **196**, 13-24 (2011).
[3] R.Z Hu., H.Liu, M.Q.Zeng, Liu J.W., M.Zhu, Chin. Sci. Bull. **57** (9). 4119-4130 (2012).
[4] A.R. Kamali, D.J. Fray, Rev., Adv. Mater.Sci. **27**, 14-24 (2011).
[5] H. Zhao, C. Jiang, X. He, J. Ren, J. Power Sourc. **184**, 532-537 (2008).
[6] R. Yazami, Nanomaterials for lithium-ion batteries: Fundamentals and applications, Pan Stanford Publishing, Singapore, 2014.
[7] A. Brenner, Electrodeposition of alloys. Principles and practice., Washington, 1963.
[8] Y. N. Sadana, J. P.Singh , R. Kumar, Surf. Technol. **24**, 319-353 (1985).
[9] S.S.A.E. Rehim, A. Awad, A.E. Sayed, J. Appl. Electrochem. **17**, 156-164 (1987).
[10] A. Gyozova, I. Krastaev, L. Petkov, T. Dobrovolska, Bulg. Chem. Comm. **48B**, 103-108 (2016).
[11] L. Zaraska, G.D. Sulka, M. Jaskuła, Technologies and Design (Kyiv National University of Technology and Design) **3** (4) 1-7 (2012).
[12] G.I. Medvedev, N.A. Makrushin, N.Y. Fursova, Russ. J. Appl. Chem. **74** (9), 1465-1469 (2001).
[13] G.I. Medvedev, S.S. Kruglikov, N.Y. Fursova, Russ. J. Appl. Chem. **74** (11) 1817-1820 (2001).
[14] W. Yang, H. Cang, Y. Tang, J. Wang, Y. Shi, J. Appl. Electrochem. **38**, 537-542 (2008).
[15] Z. Su, C. Xu, Y. Hua, J. Li, J. Ru, M. Wang, L. Xiong, Y. Zhang, Int. J. Electrochem. Sci. **11**, 3325-3338 (2016).
[16] E. Rudnik, G. Włoch, Appl. Surf. Sci. **265**, 839-849 (2013).
[17] E. Rudnik, Ionics **19** (7), 1047-1059 (2013).
[18] E. Rudnik, G. Włoch, A. Czernecka, Arch. Metall. Mater. **59** (1). 193-196 (2014).
[19] E. Rudnik, J. Electroanal. Chem. **726**, 97-106 (2014).
[20] B. Lothenbach, M. Ochs, H. Wanner, M. Yui, Thermodynamic data for the speciation and solubility of Pd, Pb, Sn, Sb, Nb and Bi in aqueous solution, Japan Nuclear Cycle Development Institute, 1999.
[21] M. Pourbaix, Atlas of electrochemical equilibria in aqueous solutions, Pergamon Press, 1966.
[22] A. Survila, Z. Mockus, S. Kanapeckaite, G. Stalnionis, J. Electroanal. Chem. **667**, 59-65 (2012).
[23] L.G. Sillen, A.E. Martell, Stability constants of metal-ion complexes. Suppl. 1, Alden Press, Oxford, 1971.
[24] E. Budevski, G. Staikov, W.J. Lorenz, Electrochemical phase formation and growth, VCH, Weinhheim, 1996.
[25] B. Sharifker, G. Hills, Electrochim. Acta **28** (7), 879-889 (1983).
[26] O. Díaz-Morales, J. Mostany, C. Borrás, B.R. Scharifker, J. Solid. State. Electrochem. **17**, 345-351 (2013).